

PAPER

# Energy gap opening by crossing drop cast single-layer graphene nanoribbons


To cite this article: Toyo Kazu Yamada *et al* 2018 *Nanotechnology* **29** 315705

View the [article online](#) for updates and enhancements.

## Related content

- [Tuning the electrical property of a single layer graphene nanoribbon by adsorption of planar molecular nanoparticles](#)  
Reetu Raj Pandey, Minoru Fukumori, Amin TermeHYousefi et al.
- [The role of defects and doping in 2D graphene sheets and 1D nanoribbons](#)  
Humberto Terrones, Ruitao Lv, Mauricio Terrones et al.
- [Temperature control of the growth of iron oxide nanoislands on Fe\(001\)](#)  
Toyo Kazu Yamada, Yuki Sakaguchi, Lukas Gerhard et al.

# Energy gap opening by crossing drop cast single-layer graphene nanoribbons

Toyo Kazu Yamada<sup>1,2</sup> , Hideto Fukuda<sup>1</sup>, Taizo Fujiwara<sup>3</sup>, Polin Liu<sup>3</sup>, Kohji Nakamura<sup>4</sup>, Seiya Kasai<sup>5</sup>, Amadeo L Vazquez de Parga<sup>6,7</sup> and Hirofumi Tanaka<sup>3</sup>

<sup>1</sup> Department of Materials Science, Chiba University, 1-33 Yayoi-cho, Inage-ku, Chiba 263-8522, Japan

<sup>2</sup> Molecular Chirality Research Center, Chiba University, 1-33 Yayoi-cho, Inage-ku, Chiba 263-8522, Japan

<sup>3</sup> Graduate School of Life Science and Systems Engineering, Kyushu Institute of Technology (Kyutech), 2-4 Hibikino, Wakamatsu, Kitakyushu 808-0196, Japan

<sup>4</sup> Department of Physics Engineering, Mie University, 1577, Kurimamachiya-cho Tsu, Mie, 514-8507, Japan

<sup>5</sup> Research Center for Integrated Quantum Electronics, Hokkaido University, North 13, West 8, Sapporo 060-8628, Japan

<sup>6</sup> Dep. Fisica de la Materia Condensada and IFIMAC, Universidad Autonoma de Madrid, Cantoblanco, 28049 Madrid, Spain

<sup>7</sup> Instituto Madrileño de Estudios Avanzados en Nanociencia IMDEA-Nanociencia, Cantoblanco 28049, Madrid, Spain

E-mail: [toyoyamada@faculty.chiba-u.jp](mailto:toyoyamada@faculty.chiba-u.jp)

Received 18 January 2018, revised 1 May 2018

Accepted for publication 9 May 2018

Published 1 June 2018



CrossMark

## Abstract

Band gap opening of a single-layer graphene nanoribbon (sGNR) sitting on another sGNR, fabricated by drop casting GNR solution on Au(111) substrate in air, was studied by means of scanning tunneling microscopy and spectroscopy in an ultra-high vacuum at 78 K and 300 K. GNRs with a width of  $\sim 45$  nm were prepared by unzipping double-walled carbon nanotubes (diameter  $\sim 15$  nm) using the ultrasonic method. In contrast to atomically-flat GNRs fabricated via the bottom-up process, the drop cast sGNRs were buckled on Au(111), i.e., some local points of the sGNR are in contact with the substrate ( $d \sim 0.5$  nm), but other parts float ( $d \sim 1-3$  nm), where  $d$  denotes the measured distance between the sGNR and the substrate. In spite of the fact that the nanoribbons were buckled,  $dI/dV$  maps confirmed that each buckled sGNR had a metallic character ( $\sim 3.5 G_0$ ) with considerable uniform local density of states, comparable to a flat sGNR. However, when two sGNRs crossed each other, the crossed areas showed a band gap between  $-50$  and  $+200$  meV around the Fermi energy, i.e., the only upper sGNR electronic property changed from metallic to p-type semiconducting, which was not due to the bending, but the electronic interactions between the up and down sGNRs.

Supplementary material for this article is available [online](#)

Keywords: graphene nanoribbon, scanning tunneling microscopy, cross structure, drop cast, energy gap

(Some figures may appear in colour only in the online journal)

## 1. Introduction

State-of-the-art nano-wiring of electronic circuits is presently based on the 14 nm Fin-FET (field effect transistor) process

[1], while the thickness of the wire for interconnects is typically larger than 30 nm and still has room for downsizing. With the use of an atomically thin wire while maintaining high conductance, downsizing the circuits in three dimensions

becomes feasible and single-layer graphene nanoribbons (sGNRs) are one of the most promising candidates [2–5]. GNRs can be fabricated by unzipping carbon nanotubes (CNTs), such that their electronic properties, e.g., the electron mean free path and the maximum allowed current density are quite similar to those of CNTs [6–9]. Although several methods have been reported to fabricate sGNRs on substrates, such as bottom-up processes [4, 5], GNRs fabricated simply by unzipping the multi-walled CNTs along the axis have been used in previous studies [10–12]. Several techniques have been reported in the last five years for unzipping CNTs through the use of (1) sulfuric acid and potassium permanganate as the oxidizing agent [11]; (2) partially embedding in a polymer film and etching by argon plasma [12]; (3) inserting alkali-metal atoms between the concentric cylinders of a multi-walled CNT [13]; (4) catalytic metal nanoparticles; and (5) gas-phase oxidation, where oxygen reacts with pre-existing defects on a CNT, forming pits, and further sonication in liquid unzips the CNT [14, 15].

In contrast to these unzipping processes, atomically-flat sGNRs grown on Au(111) were successfully fabricated by surface-assisted coupling of molecular precursors into linear polyphenylenes and their subsequent cyclodehydrogenation (i.e., bottom-up process) [4], where scanning tunneling microscopy and spectroscopy (STM/STS) have been used as powerful tools to visualize the local density of states (LDOS) of the sGNRs, and to study their dependence with the chirality of the ribbons as well as the existence of edge states [5, 16]. From a theoretical point of view the dependence of the electronic properties of the graphene nanoribbons on the edge's structure and/or the width has been addressed [17–20]. The growth of sGNRs has been explored as a feasible route to create a band gap around the Fermi level by narrowing the sGNR width (<2 nm) owing to quantization effects; so far, rectification has not been observed [17]. The electronic properties of cross-structured sGNRs are critical for the development of three-dimensional Fin-FETs.

In this manuscript, we have studied the morphology and electronic properties of sGNRs on Au(111) prepared by drop casting GNR solution by means of STM/STS in an ultra-high vacuum (UHV) at 78 and 300 K. In marked contrast to the atomically-flat sGNRs on Au(111) grown by the bottom-up process [4], our drop casting sGNRs showed unique properties. We used metallic sGNRs to explore, by means of STM/STS, the intrinsic properties of the crossing areas between two sGNRs.

We used sGNRs unzipped from a double-walled carbon nanotube (DWNT) by following the method used in the previous studies [10–12, 15], i.e., after two hours sonication, more than 95% of the DWNTs were unzipped, producing three kinds of GNRs: double-layer GNRs, Y-shaped GNRs and sGNRs. Markedly, after 16 h sonication, more than 99% of the double-layer GNRs and Y-shaped GNRs split into sGNRs, which was confirmed by Raman spectroscopy and

scanning probe microscopy [15]. We used this GNR liquid, and therefore the presence of bilayer or multilayer GNRs could be discarded in our solution. We deposited the resulting nanoribbons placing a drop of the nanoribbon solution on the Au(111) substrates. The samples were then introduced into a home-built UHV setup containing a low-temperature STM. Using a solution with a low concentration the drop casting process created a sample with individual sGNRs deposited on Au(111). The adsorbed sGNRs did not lay completely flat on the surface, some local points of the sGNR were in contact with the substrate ( $d \sim 0.5$  nm), but in other parts the sGNRs were quite far away ( $d \sim 1$ – $3$  nm) from the substrate, where  $d$  denotes distance between the adsorbed sGNR and the substrate, i.e., the sGNRs unzipped from the CNTs were buckled. The STS maps clearly show that each buckled sGNR presents metallic properties (conductance of  $\sim 3.5 G_0$ ) with a uniform LDOS, independent of the buckling. By repeatedly adding drops of the solution on the substrate, we were able to create a network of inter-crossed sGNRs, the most frequent configuration was the crossing between two sGNRs. Due to the buckling structure on the sGNR, the separation between two sGNRs was between 1.0–1.5 nm. The STS data showed uniform electronic states on the cross areas with a gap around the Fermi level of the order of 250 meV, with a lower limit of  $-50$  meV and an upper limit of  $+200$  meV i.e., the electronic properties of the sGNRs varied from metallic to p-type semiconducting.

## 2. Results and discussion

### 2.1. Imaging of drop casting sGNR on Au(111)

The sGNRs were prepared by unzipping DWNTs with careful sonication in solution such that the CNTs were carefully opened but not destroyed and thus the width of the resulting sGNRs could be controlled by the diameter of the CNTs [10–12]. In this work, we used DWNTs with diameters of 5–15 nm, i.e., the widths of the obtained sGNRs were comparable to  $\pi$  times the diameter of the unzipped CNT. Also, two carbon sheets could be initially separated by 1–2 nm, while bilayer GNRs have a separation distance of  $\sim 0.335$  nm [21]. As a substrate, we used 200 nm thick gold films deposited on mica. The films present a (111) termination with a grain size large enough to allow STM measurements in a single Au(111) crystallite [22].

Figure 1(a) shows a typical image of the surface of the Au(111) on mica, atomically-flat terraces separated by atomic steps can be observed in the STM image. The inset shows the corresponding low energy electron diffraction (LEED) pattern, the spots corresponding to the six-fold symmetry appear as small arcs due to the small rotational disorder of the different Au(111) crystallites. Figure 1(b) shows an atomically resolved STM image where the atomic periodicity of the Au(111) surface can be observed as well as the modulation

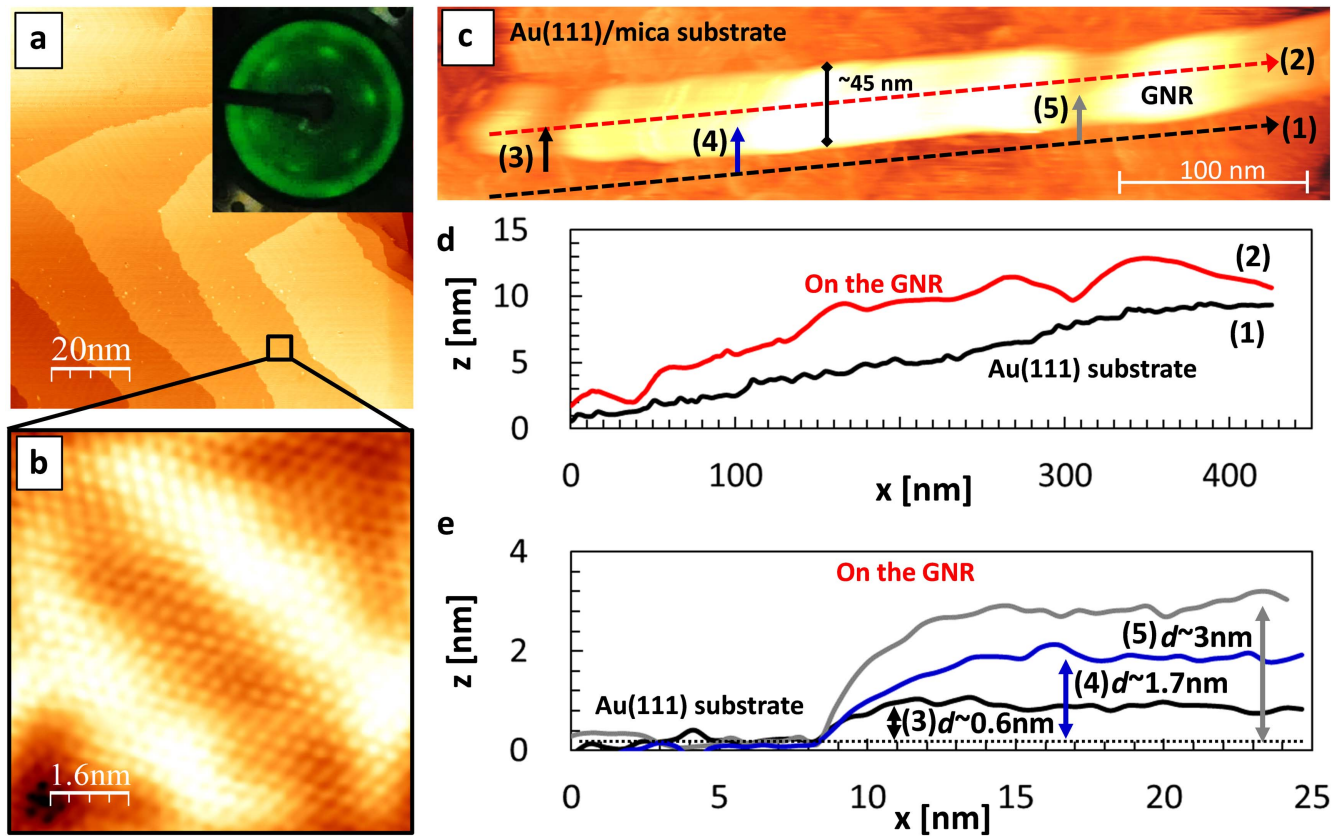


**Figure 1.** (a), (b) STM images obtained on the atomically-flat Au film ( $\sim 200$  nm thick) on mica at 78 K, which was cleaned and flattened in UHV by several cycles of  $\text{Ar}^+$  sputtering and annealing before drop casting the GNR solution. (a) Au atomic terraces ( $V_s = -1.0$  V,  $I = 50$  pA,  $100 \times 100$  nm). LEED pattern in the inset image shows six-fold fcc(111) symmetry. (b) Atomically resolved STM image of fcc-Au(111) ( $V_s = -70$  mV,  $I = 100$  pA,  $8 \times 8$  nm). Bright spheres correspond to single Au atoms, while two brighter lines correspond to the Au(111) reconstruction. (c) STM topographic image of a single-layer graphene nanoribbon (sGNR) on the Au(111) substrate ( $V_s = -1.5$  V,  $I = 50$  pA,  $475 \times 100$  nm). The width of the sGNR is  $\sim 45$  nm. (d) Line profiles along arrows (1) and (2) in (c). (e) Line profiles along arrows (3), (4) and (5) in (c).

due to the herringbone reconstruction [22]. First, we used a low concentration solution in order to deposit individual sGNRs and characterize their properties. Figure 1(c) shows an STM image ( $475 \times 100$  nm) showing a single sGNR deposited on the Au(111) surface, the width of the observed sGNR was of the order 45 nm, as expected from the diameter of the original CNTs. The line profile (1) in figure 1(d) is measured along the arrow (1) in figure 1(c) and shows a steady increase in height from left to right. The Au(111) film substrate was atomically-flat as shown in figure 1(a), but the terrace width was rather small: 10–20 nm, therefore about 30 steps exist on the substrate from left to right in the STM image in figure 1(c), generating a height difference of  $\sim 6$  nm. A single GNR was gently dropped on this substrate, producing a unique shape. In figure 1(d), the line profile (2) obtained on top the sGNR shows a different evolution with the lateral position indicating that the sGNR did not follow the morphology of the substrate. In fact, sGNR along arrow (2) shows clear buckling. Line profiles along the arrows (3)–(5) in figure 1(c) show the separation distance from the substrate (see figure 1(e)). Clearly, the separation distance changed at different positions: the shortest length  $d \sim 0.6$  nm to the longest length of  $d \sim 3$  nm, suggesting that the sGNR

was in local contact with the substrate, but in most of the areas was far away from the Au(111) substrate. We also observed that an sGNR hung on a substrate hole, i.e. an sGNR was able to float from the substrate (see the supplementary information, figure S1 is available online at [stacks.iop.org/NANO/29/315705/mmedia](https://stacks.iop.org/NANO/29/315705/mmedia).) We can speculate that this configuration may have been due to the drop casting procedure and the subsequent annealing process, because the graphene nanoribbons synthesized *in situ* always lay flat on the surface [4, 5].

## 2.2. Electronic properties of drop casting sGNRs

By means of STS we studied the electronic properties of individual sGNRs. Figure 2(a) shows the spectroscopy results measured on individual sGNRs, the  $dI/dV$  curves shown are obtained at the A, B, C, D, E, and F areas in figure 4(a). It should be noted that all curves have identical shapes and features irrespective of the position they were measured on the buckled sGNRs. In the vicinity of the Fermi energy ( $V_s \sim 0$ ),  $dI/dV$  increased linearly for both negative and positive voltages and did not reach zero at zero energy, indicating a metallic behavior as expected from the width

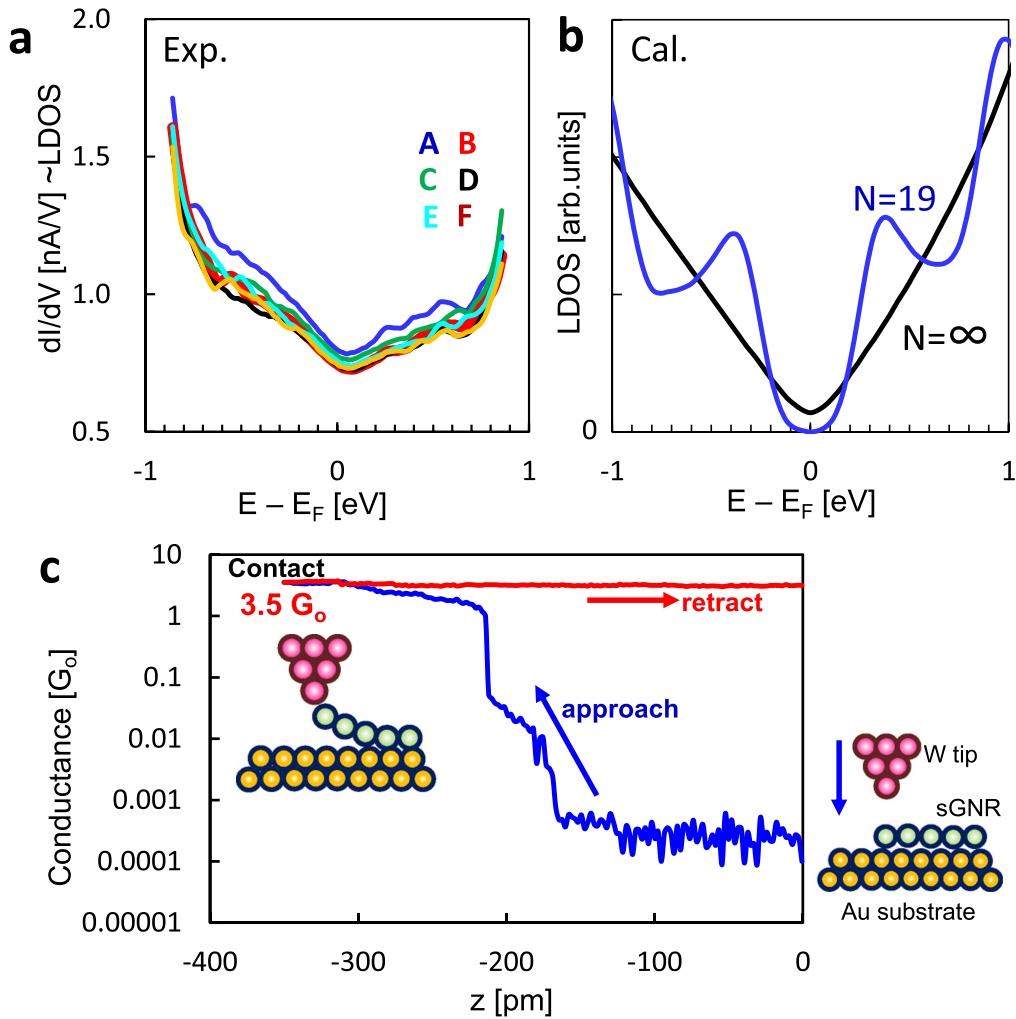


**Figure 2.** (a)  $dI/dV$  curves, proportional to the LDOS, obtained on the sGNR adsorbed on Au substrate at the areas marked by A, B, C, D, E, and F in figure 4(a). (b) Calculated LDOS of sGNR with a width of  $N = 19$  and  $N = \infty$  (see the supplementary information, figure S3). (c) STM conductance measurement through an sGNR at 78 K.  $z$  denotes the distance of the tip approaching toward the sGNR. Before approaching the STM W tip towards the sGNR on the Au substrate, the tip height position was set as  $V_s = +10$  mV,  $I = 150$  pA. The blue line shows conductance during approach. From  $-180$  pm to  $-220$  pm, we can observe big jumps of the conductance, and around  $-300$  pm, the conductance becomes constant. When we retracted the tip, the conductance was constant ( $\sim 3.5 G_0$ ), indicating that the tip is still in contact with the sGNR and the tip started to pick up the sGNR. The conductance through the partially lifted sGNR was  $\sim 3.5 G_0$ .

[17–20]. The calculated LDOS of a graphene sheet ( $N = \infty$ ) and that of an sGNR with a width of  $N = 19$ , where  $N$  represents the number of atoms included in the GNR width, are also shown in figure 2(b). Although the finite size effect in the sGNR, as seen in that of  $N = 19$ , may have opened an energy gap at the Fermi level, this happened for widths much smaller than the widths of the nanoribbons deposited in our experiments, and therefore, the experimentally observed  $dI/dV$  curves agree well with the behavior expected from the theoretical calculations. In order to test if the observed metallic behavior in the STS spectra was an intrinsic property of the deposited sGNRs or, on the contrary, we measured the metallic character of the Au(111) substrate through the graphene nanoribbon; we measured the electrical conductance along the nanoribbons' axis in contact with the STM tip at one end of the sGNRs and lifted them from the surface [23, 24]. The experimental procedure was as follows,

we approached the W tip towards the sample to make direct contact with the sGNRs avoiding plastic deformation of the sample. During the approach-retract process, the current was measured as a function of the tip-sample separation ( $I$ - $z$  curve) while the bias voltage was fixed at  $+10$  mV. The results are shown in figure 2(c), during the approach of the STM tip towards the sGNR, the tunneling current increased exponentially until the point of contact, at this point the current suddenly jumped and a constant value of conductance of  $\sim 3.5 G_0$  was obtained, a further tip approach did not change this value. It is worth mentioning that this value is comparable to the conductance of a 200 nm-long (and 14 nm-wide) sGNR ( $\sim 3 G_0$ ) [14]. We measured the STM images of the contacted sGNRs before and after the contact to check the morphology and no changes were observed. The conductance measurements are clear evidence of the metallic character of the deposited sGNRs on the Au(111) substrate.

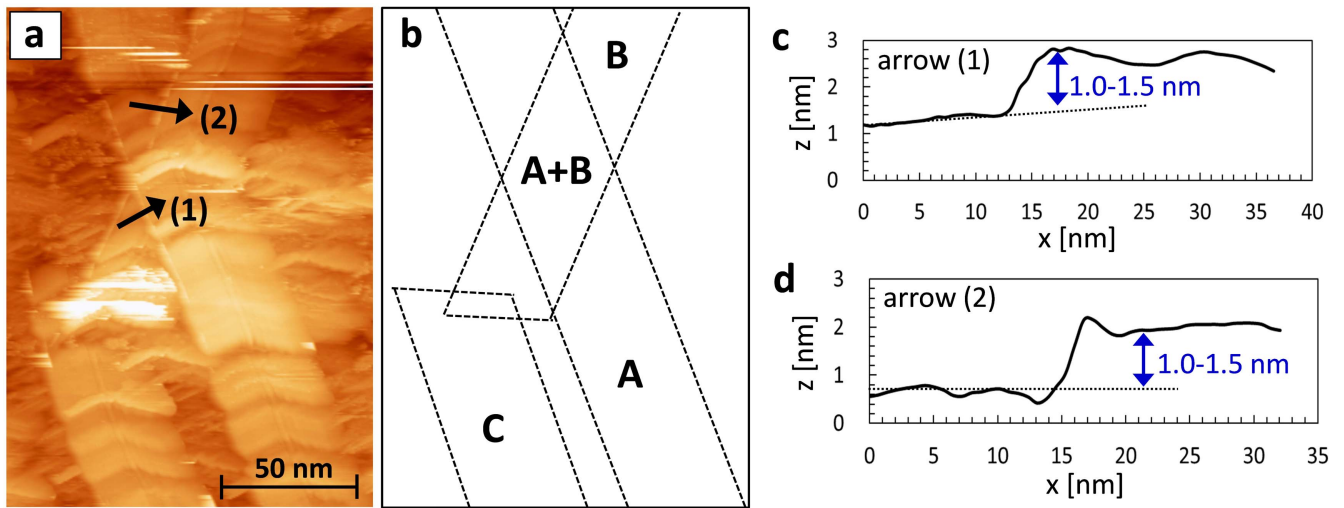


**Figure 3.** (a) STM image of cross bridging structures of sGNRs ( $V_s = -1.5$  V,  $I = 40$  pA,  $130 \times 180$  nm). Three sGNRs are stacked. (b) A simple sketch of three sGNRs in (a), named A, B, and C. Dashed lines are guides to see each sGNR. The cross bridging area is marked as A + B. (c), (d) Line profiles along the arrows (1) and (2) in (a).

### 2.3. Crossing sGNRs by drop cast

By repeating the drop casting on the same substrate, we increased the number of deposited sGNRs and therefore increased the number of sGNRs crossing each other. Figure 3(a) shows the area where three sGNRs (named A, B and C) overlapped. Figure 3(b) is a simple sketch to identify the sGNRs' positions. By comparing figures 3(a) and (b), we can see that sGNR A and B crossed. The crossing area is marked as A + B. The line profiles along arrow (1) and (2) in figure 3(a) show that the distance between the two sGNRs was always around 1.0–1.5 nm (see figures 3(c) and (d)), so the sGNRs did not lay flat one on top of the other as a consequence of the deposition method. (A wide scan range STM image is shown in the supplementary information, figure S2, where more than 20 sGNRs are stacked.)

Figure 4(a) shows an STM topographic image ( $200 \times 180$  nm) acquired in another area showing six sGNRs which are marked by numbers: 1–6. There are four sGNRs (1–4) running from left to right and another two sGNRs (5 and 6) running from the bottom to the top of the image. With this configuration GNRs 5 and 6 partially crossed with GNRs 1–4. The crossed areas are marked by G1 and G2. Simultaneously to the topographic image we measured at every pixel of the image the  $dI/dV$  curve. Figure 4(b) shows the  $dI/dV$  map at +30 meV. The brighter color denotes higher  $dI/dV$  [nA/V], i.e. a higher LDOS. By comparing figures 4(a) and (b), we conclude that sGNRs 1–4 show uniform signal in the  $dI/dV$  map, which confirms that monolayer sGNRs present a uniform LDOS as long as they are deposited on the Au(111) substrate, as discussed before. However, in all the areas where two sGNRs cross the  $dI/dV$  signal is smaller and the areas appear darker in the maps, i.e., there is a clear reduction in the LDOS of the nanoribbons in comparison to the ones deposited on Au(111). Figures 4(c) and (d) show the line profile along the arrows in the topographic image (figure 4(a)) and the  $dI/dV$

map at +30 mV (figure 4(b)), respectively. Since the sGNR surface was not flat, the line profile in figure 4(c) shows height variations within GNR 3. At the position where GNR 3 crossed with GNR 5, the height changed by  $\sim 1.0$  nm, which agrees with the average distance measured in the other overlapping areas (see figure 3). On the other hand, the line profile in the  $dI/dV$  map along the same path gives us interesting information (figure 4(d)). In spite of the fact that the topographic height varied along GNR 3, the  $dI/dV$  values remain constant around  $0.20 \pm 0.05$  nA V $^{-1}$ , i.e., the LDOS inside the GNR are quite uniform, independent of the morphology variation. The  $dI/dV$  curves obtained at the A–F areas in figure 4(a) are shown in figure 2(a). It should be noted that all curves show similar features, i.e., in the vicinity of the Fermi energy ( $V_s \sim 0$ ),  $dI/dV$  increases linearly for both negative and positive voltages, meaning that the LDOS at different positions on the sGNRs is almost the same. Markedly, at the position where the two sGNRs overlap, the  $dI/dV$  signal rapidly dropped down to  $\sim 0.0$  nA/V, and remained constant in all the crossing areas. The edge of the crossing area is focused on in figure 4(e), where the height variation of 1.0 nm takes place in  $\Delta \sim 7$  nm distance, however, the  $dI/dV$  signal drops within  $\Delta \sim 3$  nm, which indicates that the  $dI/dV$  drop was not due to the GNR bending, but the electronic interactions between the up and down sGNRs. Figure 4(f) shows the  $dI/dV$  curve obtained at the crossed area (G1 in figure 4(a)), it presents  $dI/dV$  values of  $\sim 0.00$  nA/V around the Fermi energy (red curve). The blue curve in figure 4(e) was obtained from the crossed sGNR area at G2 in figure 4(a) where GNRs 2 and 6 cross each other. It should be noted that G1 and G2 crossing areas showed exactly the same  $dI/dV$  curve, i.e., different crossed sGNRs had the same LDOS and gap, suggesting that there was no crossing angle dependence between two sGNRs, further suggesting that random stacking sGNRs may have a gap. Just by crossing, the sGNRs changed their electronic property from metallic to semiconducting.

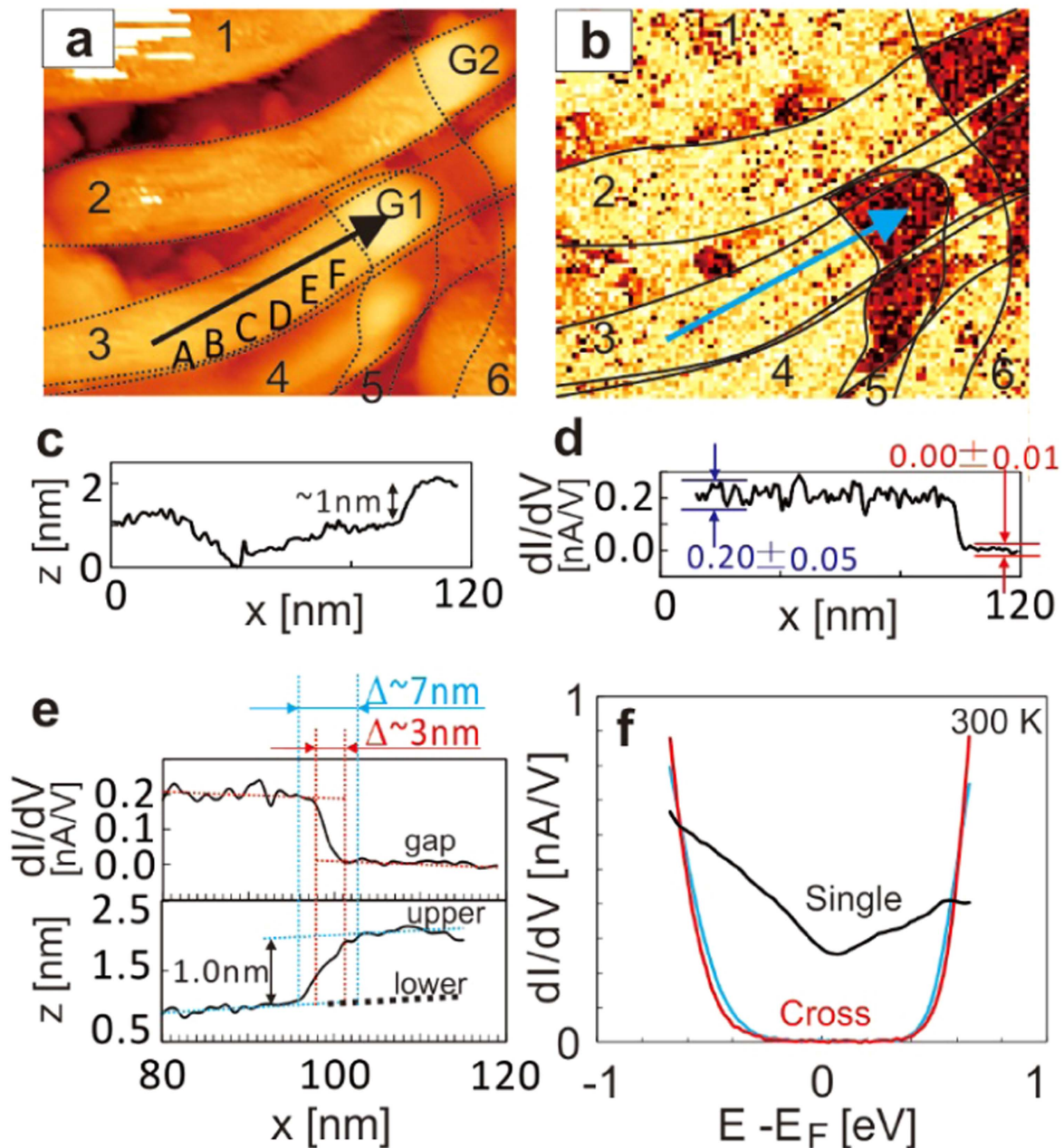


**Figure 4.** (a) STM topographic image of sGNRs on the Au(111) substrate ( $V_s = -1.0$  V,  $I = 500$  pA,  $200 \times 180$  nm). Six sGNRs are observed. Four sGNRs marked by 1, 2, 3, and 4 run from left to right, while 5 and 6 run from the bottom to the top of the image. Areas marked with G1 and G2 indicates zones where the two GNRs overlap. (b)  $dI/dV$  map at +30 mV obtained at the same area as (a). Brighter color denotes high density of states. (c) Line profile along the arrow in (a). The crossing sGNRs show a height difference of  $\sim 1.0$  nm. (d) Line profile in the  $dI/dV$  map along the arrow shown in (b). (e) Enlarged plots in (c) and (d). (f)  $dI/dV$  curves obtained at 300 K on the sGNR (black line) and on the area G marked in (a). Red and blue curves are obtained from the areas marked by G1 and G2 in panel (a), respectively.

In order to characterize with precision the energy position of the gap we measured  $dI/dV$  curves with high energy resolution. Figure 5(a) shows  $dI/dV$  maps at  $-697$ ,  $+10$ ,  $+313$ , and  $+717$  mV obtained at the boundary between the sGNR and the crossed GNRs. At  $-697$  mV, it is hard to see the difference in the map, meaning the sGNR and the crossed sGNRs had a comparable conductance, however, at  $+10$  mV, the crossed sGNRs show clear dark contrast, while the contrast becomes weaker with an increase in the bias (see the map at  $+313$  mV), and finally at  $+717$  mV even the crossed area

appears brighter. These variations in the differential conductance maps can be clearly explained by the  $dI/dV$  plot on a log-scale shown in figure 5(b). White and red dots are the  $dI/dV$  plots obtained at the sGNR and the crossed sGNRs, respectively. Around  $-650$  meV, both the sGNR and crossed sGNRs have a similar conductance of  $\sim 0.5$  nA/V, then from  $-650$  meV to  $-50$  meV, the conductance of the crossed sGNRs drastically decays below  $0.01$  nA/V. Above  $+200$  meV, again the conductance of the crossed sGNRs starts to increase rapidly and above  $\sim +600$  meV, the

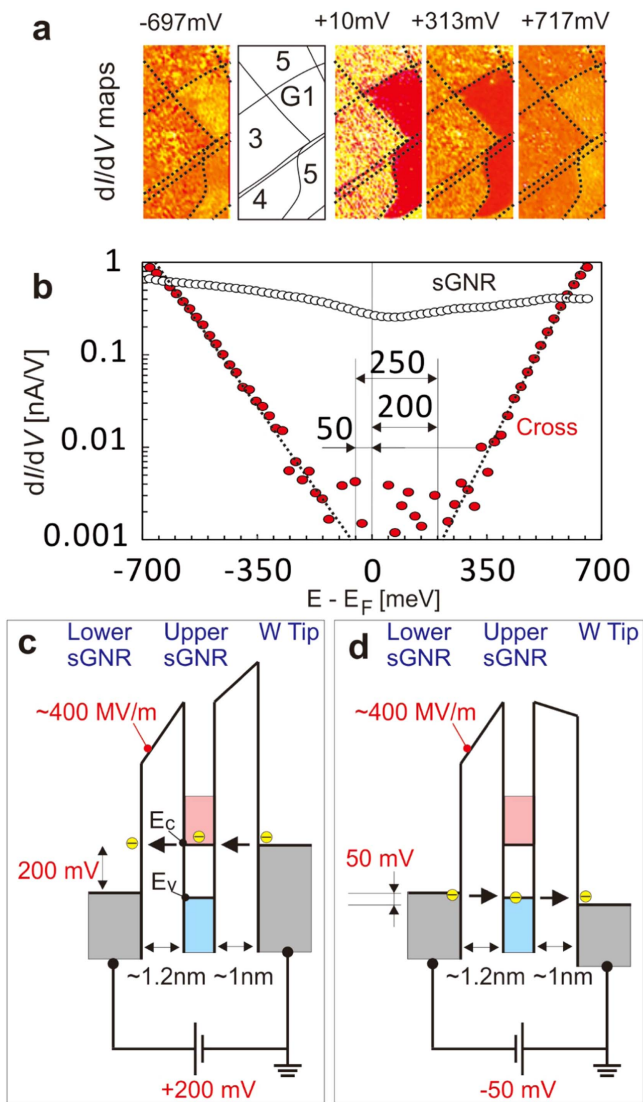


**Figure 5.** (a)  $dI/dV$  maps at  $-697$ ,  $+10$ ,  $+313$ , and  $+717$  mV obtained from the crossed sGNRs areas. Brighter areas denote higher conductance. (b) Differential conductance ( $dI/dV$ ) plot on a log-scale as a function of energy, where zero corresponds to the Fermi energy, and positive and negative energy denote unoccupied and occupied states, respectively. White and red dots show  $dI/dV$  values obtained on the sGNR area and the crossed sGNRs area, respectively. Two dashed lines denote the region where  $dI/dV$  values are lower than  $0.002 \text{ nA V}^{-1}$ , suggesting a band gap. (c), (d) Scheme showing the electron transfer between the tip and the sample at the crossed sGNRs areas. From the left side, the lower sGNR/Au(111) substrate, the upper sGNR, and the W tip energy diagrams are shown. Bias voltage is applied between the substrate and the tip. The substrate and the upper sGNR are separated by  $\sim 1.2 \text{ nm}$ , and the W tip and the upper sGNR are separated by  $\sim 1 \text{ nm}$ . In (c), a positive bias voltage of  $+200 \text{ mV}$  and, in (d), a negative bias voltage of  $-50 \text{ mV}$  is applied.  $E_c$  and  $E_v$  denote conduction and valence band edge, respectively.

conductance of the crossed sGNRs becomes higher than that of the sGNR. From this plot, if we define the  $dI/dV$  values lower than  $0.002 \text{ nA/V}$  as insulating, we can say that the crossed sGNRs have a gap between  $-50$  and  $+200 \text{ meV}$  around the Fermi energy (an energy gap width of  $E_g = 250 \text{ meV}$ ), i.e., the crossed sGNRs have p-type semiconducting characteristics.

There are a couple of mechanisms that could explain the presence of a gap in the LDOS of the upper GNRs in the overlapping areas. Botello-Mendez *et al* calculated that the stacking angle between individual GNRs plays a central role in dictating the probability of transmission of the electrons from one ribbon to the other [21]. In fact, gaps were found in perpendicular conductance at crosses with different orientations. Initially one can think that our STM/STS results agree with these theoretical predictions; however, a detailed analysis of our results indicates that the presence of a gap in the differential conductance must have a different origin. On the one hand, in our experiments, the gap width in the conductance does not depend on the angle between the crossing ribbons, as opposed to the calculations. On the other hand, our experiments measured the tunnel probability when the STM tip was located on top one of the crosses of the graphene nanoribbons and not directly the probability of transmission of an electron from the upper to the lower nanoribbon. The GNRs used in this study are metallic, as demonstrated above, and therefore even if the transmission of electrons between the upper and lower ribbon is prohibited, we should not see a gap in the differential tunneling conductance measured by means of STM since the electrons can reach the Au(111) by moving through the top ribbon.

An alternative explanation for our experimental results is the existence of a gap in the electronic structure of graphene bilayers. It has been shown that breaking the inversion symmetry in graphene bilayers by applying an electric field perpendicular to the plane of the graphene bilayer opens a gap [25, 26]. A similar way of getting the same results is growing or depositing the bilayer on a substrate, which modifies the density of carriers differently in one of the layers of the bilayer [9, 27]. In all cases gaps observed are of the order  $250 \text{ mV}$ . Figures 5(c) and (d) show schematics of electron transfer between the tip and the sample when positive ( $+200 \text{ mV}$ ) and negative ( $-50 \text{ mV}$ ) bias voltages are applied. At the crossed structure, upper and lower sGNR layers were stacked. We know that the lower sGNR layer has a metallic property, thus electrons fill up to the Fermi energy ( $E_F$ ). However, the situation of the upper sGNR layer is totally different; from the STS results in figures 5(a) and (b), we know that the LDOS of the upper sGNR layer has a gap. In figures 5(c) and (d), blue and red lines denote the valence band edge ( $E_v$ ) and the conduction band edge ( $E_c$ ) of the upper sGNR layer, respectively. When a positive bias was applied to the sample, electrons from the tip Fermi energy tunneled into the unoccupied states of the sample substrate through the conduction band of the upper sGNR layer (see figure 5(c)). Reversely, when a negative bias was applied to the sample, electrons tunneled from the Fermi energy of the substrate to the tip unoccupied states through the valence band of the upper sGNR layer. Considering that Fermi levels in the lower GNR and the Au substrate were in equilibrium whereas the upper sGNRs was electrically isolated from the lower one by  $1.0 \text{ nm}$  spacing, the vertical electric field of around  $400 \text{ MV m}^{-1}$  could have been caused between the two sGNRs layers by the difference in work functions of Au and the sGNR;  $5.1 \text{ eV}$  for Au and  $4.7 \text{ eV}$  for



graphene [28]. It is worth mentioning that the STM tip potential hardly influenced the electric field in the sGNRs due to the presence of the metallic substrate. In fact, we did not find any dependence of the measured width of the energy gap with the tunneling current used during the measurements.

### 3. Materials and methods

#### 3.1. STM setup

All experimental studies were performed with home-built UHV-STM equipment [29], which consists of introduction, preparation, and analytical chambers. The scanning head of the equipment was located inside the analytical chamber and was cooled down to low temperatures with a cryostat. We achieved 78 K by filling liquid nitrogen (LN<sub>2</sub>) in the cryostat (4 liters of LN<sub>2</sub> remained at 78 K for more than 80 h). W tips were fabricated by chemical etching from a commercial polycrystalline W wire (99.9% purity) with KOH aq. under air. The etched W tip apices were quickly checked by SEM (Technex Tiny-SEM,  $\sim 10^{-3}$  Pa). Sharp tips were subsequently introduced into the UHV-STM setup. In the preparation chamber, the tip apex was properly annealed by electron bombardment (10–30 W, 10 s, once) to remove oxide layers coating the apex [30], then without breaking UHV, the tip was set into the STM.

#### 3.2. STM spectroscopy

All STM topographic images were obtained in constant-current mode using a feed-back loop. With the use of STM spectroscopy, the LDOS of each atomic position could be directly obtained [29, 31–33]. The tunneling current as a function of the sample bias voltage ( $I$ - $V$  curve) was measured at each pixel position in the STM topographic image. The differential conductance ( $dI/dV$ ) was obtained by numerical differentiation of the  $I$ - $V$  curve. Since the experimentally obtained  $dI/dV$  is proportional to the sample LDOS [29, 31–34], the zero voltage corresponded to the Fermi energy and  $dI/dV$  in the positive (negative) voltage range denoted the unoccupied (occupied) state. Conductance through the sample could also be measured by approaching the W tip to the sample to make direct contact without plastic deformation of the sample [23, 24]. During the approach-retract process, the current was measured as a function of the tip-sample separation ( $I$ - $z$  curve). We set the constant voltage at +10 mV during the  $I$ - $z$  measurement. Typically, the tip detected the tunneling current increasing exponentially when the tip started to approach the sample. The current (and thus the conductance) was drastically increased by a factor of more than 10 when the tip made contact with the sample. Further approaching the sample did not significantly increase the current. Here, we used  $G_0 = 2e^2/h \sim 1/12.9$  k $\Omega$  [23, 24], where  $e$  is electron charge, and  $h$  is Planck's constant.

#### 3.3. Au(111)/mica substrates

Commercial Au films ( $\sim 200$  nm thick) deposited on mica were used as substrates. The observation of atomically-flat sGNRs required atomically-flat substrates. In the present study, we used two methods: (1) the Au/mica was heated in air by flame for 5 s (we used the top of the orange-flame, C<sub>4</sub>H<sub>10</sub> gas). (2) the Au/mica was sputtered by Ar<sup>+</sup> (+1 kV, 10 min) and annealed (853 K) in the UHV preparation chamber. We repeated these cycles five times (too much sputtering removes the entire Au film). LEED located inside the preparation chamber showed six-fold fcc-Au(111) spots. STM topographic images showed atomically-flat terraces.

#### 3.4. GNR preparation

First, the atomically-flat Au(111) substrates were confirmed in our STM setup, and then the substrate was taken out of the setup. GNRs were produced by unzipping the DWNTs in liquid [10–12, 15]. Under sonication (37 kHz, 600 W) for 2 h, more than 95% of the DWNTs were unzipped, producing double-layer GNRs ( $\sim 20\%$ ), Y-shaped GNRs ( $\sim 30\%$ ), and sGNRs ( $\sim 45\%$ ) (see the supplementary information in ref. [15]). Further sonication for more than 16 h split more than 99% of the double-layer GNRs and Y-shaped GNRs into sGNRs. We used this solution in this study. The sGNR liquid was drop cast at the center of the substrate under air. The size of the substrate was  $10 \times 5$  mm<sup>2</sup> with a thickness of  $\sim 0.5$  mm. The sample was then annealed up to 623 K for 3 h in air to remove poly (*m*-phenylene vinylene-co-2,5-dioctoxy-*p*-phenylene) (PmPV). Again, the sample was set into the UHV setup, and annealed in the preparation chamber at 853 K for 10–30 min. The sample was transferred to the analytical chamber and we performed the STM/STS measurements.

#### 3.5. Theoretical calculations

As a theoretical model of the GNR, we adopted an armchair ribbon with a width of  $N$  atomic rows of carbon, where both edges were terminated by hydrogens to remove the effects of the dangling bonds (see the supplementary information, figure S3). The bond length was taken to be the experimental value of graphite, 0.142 nm. Calculations were performed based on the local spin density approximation using the full-potential linearized augmented plane-wave method with a single slab geometry [35–37]. Linearized augmented plane-wave functions with a cutoff of  $|k+G| < 5.0$  a.u.<sup>-1</sup> and muffin-tin (MT) sphere radii of 1.2 and 0.8 a.u., respectively, were used for the C and H atoms, where the angular momentum expansions inside the MT spheres were truncated at 1, 6 and 4 for the wave functions, charge density, and potential.

### 4. Conclusion

In this study, single-layer metallic graphene nanoribbons unzipped from double-walled carbon nanotubes with a sonication method were deposited on Au(111) by drop casting the sGNR solution in air with subsequent annealing (853 K) in

UHV. In contrast to the bottom-up CVD process, the drop cast sGNRs were buckled, i.e., some local points of the sGNR were in contact with the substrate ( $d \sim 0.5$  nm), but other parts were further apart ( $d \sim 1\text{--}3$  nm). The STS maps clearly showed that single buckled sGNRs on Au(111) have metallic properties (conductance of  $\sim 3.5 G_0$ ) with considerable uniform LDOS, independent of topographic variations. On the contrary, the areas where two sGNRs overlapped show a uniform electronic structure with an energy gap between  $-50$  and  $+200$  meV around the Fermi energy, i.e., the electronic properties of the sGNRs varied from metallic to p-type semiconducting, which was not due to the bending, but the electronic interactions between the up and down sGNRs. These findings in our STM/STS studies of the crossed sGNRs could be useful with regard to future architecture of cross bridging array structures in nanodevices using sGNRs.

## Acknowledgments

This work was supported by JSPS KAKENHI Grant numbers 23681018, 25110011, 15H03531, 25110002, 25110013 and 16K05415, the Asahi Glass Foundation, and the Spanish Ministry of Economy and Competitiveness through Grants FIS2015-67367-C2-1-P and the Comunidad de Madrid through Grant MAD2D-CM. We thank Dr L Gerhard, Dr E Inami, and Mr N M K Nazriq for their careful reading of our manuscript, and Mr M Shimasaki for his support of the Au(111) substrate preparation. Computations were performed at the Research Institute for Information Technology, Kyushu University, and Supercomputer Center, Institute for Solid State Physics, University of Tokyo.

## ORCID iDs

Toyo Kazu Yamada  <https://orcid.org/0000-0001-5185-6472>

## References

- [1] The International Technology Roadmap for Semiconductors (ITRS) 2013 Edition
- [2] Chen Z, Lin Y-M, Rooks M J and Avouris P 2007 Graphene nano-ribbon electronics *Physica E* **40** 228–32
- [3] Behnam A, Johnson J L, An Y, Biswas A and Ural A 2011 Electronic transport in graphitic nanoribbon films *ACS Nano* **5** 1617–22
- [4] Cai J *et al* 2010 Atomically precise bottom-up fabrication of graphene nanoribbons *Nature* **466** 470–3
- [5] Ruffieux P *et al* 2012 Electronic structure of atomically precise graphene nanoribbons *ACS Nano* **6** 6930–5
- [6] Berger C *et al* 2004 Ultrathin epitaxial graphite: 2D electron gas properties and a route toward graphene-based nanoelectronics *J. Phys. Chem. B* **108** 19912–6
- [7] Obradovic B, Kotlyar R, Heinz F, Matagne P, Rakshit T, Giles M D, Stettler M A and Nikonov D E 2006 Analysis of graphene nanoribbons as a channel material for field-effect transistors *Appl. Phys. Lett.* **88** 142101
- [8] Berger C *et al* 2006 Electronic confinement and coherence in patterned epitaxial graphene *Science* **312** 1191–6
- [9] Ohta T, Bostwick A, Seyller T, Horn K and Rotenberg E 2006 Controlling the electronic structure of bilayer graphene *Science* **313** 951–4
- [10] Terrones M 2009 Nanotubes unzipped *Nature* **458** 845–6
- [11] Kosynkin D V, Higginbotham A L, Sinitskii A, Lomeda J R, Dimiev A, Proce B K and Tour J M 2009 Longitudinal unzipping of carbon nanotubes to form graphene nanoribbons *Nature* **458** 872–6
- [12] Jiao L, Koshang Z L, Wang X, Diankov G and Dai H 2009 Narrow graphene nanoribbons from carbon nanotubes *Nature* **458** 877–80
- [13] Cano-Marquez A G *et al* 2009 Ex-MWNTs: graphene sheets and ribbons produced by lithium intercalation and exfoliation of carbon nanotubes *Nano Lett.* **9** 1527–33
- [14] Jiao L, Wang X, Diankov G, Wang H and Dai H 2010 Facile synthesis of high-quality graphene nanoribbons *Nat. Nanotechnol.* **5** 321–5
- [15] Tanaka H, Arima R, Fukumori M, Tanaka D, Negishi R, Kobayashi Y, Kasai S, Yamada T K and Ogawa T 2015 Method for controlling electrical properties of single-layer graphene nanoribbons via adsorbed planar molecular nanoparticles *Sci. Rep.* **5** 12341
- [16] Tao C *et al* 2011 Spatially resolving edge states of chiral graphene nanoribbons *Nat. Phys.* **7** 616–20
- [17] Yang L, Park C H, Son Y W, Cohen M L and Louie S G 2007 Quasiparticle energies and band gaps in graphene nanoribbons *Phys. Rev. Lett.* **99** 186801
- [18] Han M Y, Ozyilmaz B, Zhang Y and Kim P 2007 Energy band-gap engineering of graphene nanoribbons *Phys. Rev. Lett.* **98** 206805
- [19] Avouris P, Chen Z and Perebeinos V 2007 Carbon-based electronics *Nat. Nanotechnol.* **2** 605–15
- [20] Son Y-W, Cohen M L and Louie S G 2006 Energy-gaps in graphene nanoribbons *Phys. Rev. Lett.* **97** 216803
- [21] Botello-Mendez A R, Cruz-Silva E, Rome-Herrera J M, Lopez-Urias F, Terrones M, Sumpter B G, Terrones H, Charlier J C and Meunier V 2011 Quantum transport in graphene nanonetworks *Nano Lett.* **11** 3058–64
- [22] Chidsney C H E D, Loiacono D N, Sleator T and Nakahara S 1988 STM study of the surface morphology of gold on mica *Surf. Sci.* **200** 45–66
- [23] Joachim C, Gimzewski J K, Schlittler R R and Chavy C 1995 Electronic transparency of a single C<sub>60</sub> molecule *Phys. Rev. Lett.* **74** 2102
- [24] Schmaus S, Bagrets A, Nahas Y, Yamada T K, Bork A, Evers F and Wulfhekel W 2011 Giant magnetoresistance through a single molecule *Nat. Nanotechnol.* **6** 185
- [25] Ando T and Koshino M 2009 Field effects on optical phonons in bilayer graphene *J. Phys. Soc. Jpn.* **78** 034709
- [26] Castro E V, Novoselov K S, Morozov S V, Peres N M R, Lopes dos Santos J M B, Nilsson J, Guinea F, Geim A K and Castro Neto A H 2007 Biased bilayer graphene: semiconductor with a gap tunable by the electric field effect *Phys. Rev. Lett.* **99** 216802
- [27] Zhang Y, Tang T-T, Girit C, Hao Z, Martin M C, Zetti A, Crommie M F, Shen Y R and Wang F 2007 A tunable phonon-exciton Fano system in bilayer graphene *Nat. Mater.* **459** 820
- [28] Yu Y-J, Zhao Y, Ryu S, Brus L E, Kim K S and Kim P 2009 Tuning the graphene work function by electric field effect *Nano Lett.* **9** 3430
- [29] Yamagishi Y, Nakashima S, Oiso K and Yamada T K 2013 Recovery of nanomolecular electronic states from tunneling spectroscopy: LDOS of low-dimensional phthalocyanine molecular structures on Cu(111) *Nanotechnology* **24** 395704
- [30] Yamada T K, Abe T, Nazriq N M K and Irisawa T 2016 Electron-bombarded <110>-oriented tungsten tips for stable tunneling electron emission *Rev. Sci. Instr.* **87** 033703

- [31] Yamada T K, Bischoff M M J, Heijnen G M M, Mizoguchi T and van Kempen H 2003 Observation of spin-polarized surface states on ultrathin bct Mn(001) films by spin-polarized scanning tunneling spectroscopy *Phys. Rev. Lett.* **90** 056803
- [32] Gerhard L, Yamada T K, Balashov T, Takacs A F, Daena M, Ostanin S, Ernst A, Mertig I and Wulfhekel W 2010 Magneto-electric coupling at metal surfaces *Nat. Nanotechnol.* **5** 792
- [33] Yamada T K 2015 How to get molecular spin-polarization using spin-polarized STM *J. Surf. Sci. Soc. Jpn.* **36** 375
- [34] Ukraintsev V A 1996 Data evaluation technique for electron-tunneling spectroscopy *Phys. Rev. B* **53** 11176
- [35] Wimmer E, Krakauer H, Weinert M and Freeman A J 1981 Full-potential self-consistent linearized-augmented-plane-wave method for calculating the electronic structure of molecules and surfaces: O<sub>2</sub> molecule *Phys. Rev. B* **24** 864–75
- [36] Weinert M, Wimmer E and Freeman A J 1982 Total-energy all-electron density functional method for bulk solids and surfaces *Phys. Rev. B* **26** 4571–8
- [37] Nakamura K, Ito T, Freeman A J, Zhong L and Fernandez-de-Castro J 2003 Enhancement of magnetocrystalline anisotropy in ferromagnetic Fe films by intra-atomic noncollinear magnetism *Phys. Rev. B* **67** 014420